ChemPubSoc Europe

DOI: 10.1002/chem.201902945

CHEMISTRY A European Journal Full Paper

Inorganic Materials |*Hot Paper*|

Proton Acidity and Proton Mobility in ECR-40, a Silicoaluminophosphate that Violates Löwenstein's Rule

Michael Fischer*[a, b]

Abstract: The silicoaluminophosphate zeotype ECR-40 contains linkages of AlO_4 tetrahedra via a common oxygen atom, thereby violating the famous "Löwenstein's rule". In this work, a combination of static density functional theory (DFT) calculations and DFT-based ab-initio molecular dynamics (AIMD) simulations were employed to study the acidity and mobility of protons associated with such unusual linkages. It was found that the Al-O-Al linkages are preferentially protonated, as deprotonation causes a local accumulation of negative charge. The protons at these linkages possess a somewhat lower Brønsted acidity than those at Si-O-Al links. AIMD simulations for fully hydrated ECR-40 predicted a partial deprotonation of the Al-O-Al linkages, whereas Si-O-Al linkages were fully deprotonated. Frequently, a coordination of water molecules to framework Al atoms was observed in the vicinity of the Al-O-Al links. Hence, these linkages appear prone to break upon dehydration, potentially explaining why Löwenstein's rule is mostly obeyed in materials formed in aqueous media.

Introduction

Löwenstein's rule, first postulated in 1954, states that the linkage of two AlO_4 tetrahedra via a common oxygen atom is energetically unfavourable and therefore avoided in aluminosilicates ("Al-O-Al avoidance rule").[1] While it was developed using a simple argument based on Pauling's third rule,[2] and initially illustrated with only a few examples, it is commonly assumed that Löwenstein's rule holds for most members of important groups of aluminosilicates, such as feldspars[3,4] and zeolites.[5] In addition to some general criticism regarding its theoretical foundation,[3] evidence for a violation of Löwenstein's rule has been reported for a number of aluminosilicates. For example, non-Löwenstein Al-O-Al linkages have been found to occur in the natural zeolites stilbite (Si/Al ratio of 3)[6] and analcime (Si/Al = 2),[7] in various sodalite-type compounds (where the Si/Al ratio may be smaller than one, and even pure aluminates can be synthesised),[4,8] and in the sorosilicate gehlenite (Si/Al = 1:2).[9] Two recent computational studies have re-evaluated the validity of Löwenstein's rule in zeolites. Employing density functional theory (DFT) calculations, Fletcher et al. screened various arrangements of Si and Al in the unit cell of chabazite at different Si/Al ratios (Si/Al = 17, 11, 8), as well as some other zeolite frameworks (ABW, LTA, RHO, MOR) at fixed Si/Al ratio.[10] Surprisingly, they found many cases where configurations with one or several non-Löwenstein linkages gave the lowest DFT energy, contrary to the common assumption that Al-O-Al linkages are thermodynamically unstable. Because zeolites are formed in aqueous media, a subsequent study by Heard et al. investigated the influence of water on the stability of Al-O-Al linkages in protonated chabazite (H-CHA), using a combination of DFT structure optimisations and DFT-based ab initio molecular dynamics (AIMD) calculations.[11] While their calculations predicted a non-Löwenstein configuration to be favoured in the dehydrated state, in line with the results of Fletcher et al., a configuration obeying Löwenstein's rule was favoured in hydrated models at high water loadings. A higher Brønsted acidity was found for protons associated with Si-O-Al linkages compared to those located at Al-O-Al linkages. As a consequence, the Si-O-Al linkages were found to be deprotonated in AIMD simulations of hydrated models, leading to the formation of protonated water clusters (= hydrated hydronium ions[12]) in the pores. Framework deprotonation was not observed for non-Löwenstein linkages. The ability of the protons at Si-O-Al linkages to transfer to water molecules in the pores provides an additional energetic stabilisation that is absent for Al-O-Al linkages, which could be a plausible explanation for the experimentally observed preference for arrangements obeying Löwenstein's rule.

A variety of synthetic aluminophosphates (AlPOs, composition $AlPO_4$) and heteroatom-doped AlPO derivatives (silicoaluminophosphates—SAPOs, metal aluminophosphates—

[a] *Dr. M. Fischer*
Crystallography Group, Department of Geosciences
University of Bremen, Klagenfurter Straße 2–4, 28359 Bremen (Germany)
E-mail: michael.fischer@uni-bremen.de

[b] *Dr. M. Fischer*
MAPEX Center for Materials and Processes
University of Bremen, 28359 Bremen (Germany)

Supporting Information and the ORCID identification number(s) for the author(s) of this article can be found under: https://doi.org/10.1002/chem.201902945.

MeAPOs) with zeolite-like topologies have been reported.[13–15] Such aluminophosphate-based zeotypes exhibit considerable potential for applications in catalysis,[16–18] adsorption- and membrane-based gas separations,[19–21] and thermal energy storage.[22,23] Pure AlPOs have a strictly alternating arrangement of Al and P on the T sites, as both Al-O-Al and P-O-P linkages are unstable.[15] In SAPOs and MeAPOs, the heteroatom substitution occurs in a way that unstable linkages are avoided. For example, Si is incorporated either by replacing single P atoms or by forming larger Si "islands" or aluminosilicate domains, thereby avoiding Si-O-P linkages.[24,25] There are only a few examples of AlPO-based materials in which Al-O-Al linkages are present in the crystal structure,[26] such as a layered aluminophosphate with composition $Cs_2Al_2P_2O_9$.[27] A zeotype example is the system investigated in the present work, the silicoaluminophosphate ECR-40 (ECR = Exxon Corporate Research). This material, first reported by Vaughan in 1999[28] and described in more detail by Afeworki et al. in 2004,[29] exhibits a higher acidity than most SAPOs. This property was, in part, attributed to strong Brønsted acid sites associated with the Al-O-Al linkages, an explanation that appears at least debatable in the view of the more recent computational results mentioned above.

ECR-40 has the MEI topology of the zeolite ZSM-18.[30,31] As the MEI framework contains three-, five- and seven-membered rings, a strict alternation of Al and P on the tetrahedral sites (T sites) is not possible. However, as discussed in detail in the structural analysis performed by Afeworki et al.,[29] Si-O-P linkages can be avoided if the silicon atoms occupy the T sites belonging to the three-membered rings. In ECR-40, two $3^1{\cdot}4^3{\cdot}5^3$ building units (**t-mei** tiles in the nomenclature of the natural tiling approach[32]) are fused together to form a 17 T atom unit via a common Si_3O_3 ring (Figure 1 a). Al-O-Al linkages connect the apexes of these 17 T atom units, forming infinite chains parallel to the *c*-axis. Pairs of Al-O-P linkages join the chains perpendicular to the *c*-direction (Figure 1 b), resulting in the formation of one-dimensional twelve-membered ring (12MR) channels running along *c* (Figure 1 c). These channels are connected via unusual seven-ring windows (7MR). The good agreement between theoretical and measured stoichiometry, the ranges of T–O bond distances obtained in the Rietveld refinement, and the results of solid-state NMR experiments all substantiated the assumption of an ordered distribution of Al, P, and Si on the T sites of ECR-40.[29]

The occurrence of peculiar Al-O-Al linkages in ECR-40 and related MEI-type SAPOs was explained by Hong and co-workers.[33] Using synchrotron diffraction experiments on ECR-40 samples prepared with different organic structure directing agents (OSDAs), these authors could show that the OH groups of the OSDAs are covalently bonded to the Al1 atoms in the as-synthesised material. As a consequence, the Al_1 atom is octahedrally coordinated, and two AlO_6 octahedra are joined together via a common face. The presence of AlO_6 octahedra was corroborated using solid-state NMR experiments, and further explained through in situ studies of the crystallisation mechanism. Due to the presence of an unusual covalent bond between framework T atoms and OSDA molecules, Hong and co-workers suggested to allocate ECR-40 to a new family of inorganic–organic hybrids dubbed "framework-bound OSDA-containing molecules sieves" (FOMSs). Upon OSDA removal, the face-sharing AlO_6 octahedra are converted into corner-sharing AlO_4 tetrahedra, leading to the non-Löwenstein Al1-O6-Al1 linkage that is found in the calcined structure.[29] Rehydration of the calcined form leads to the formation of AlO_6 octahedra that are sharing a common face consisting of three water molecules. The rehydrated form becomes amorphous upon recalcination, indicating instability of the Al-O-Al linkages towards repeated hydration/dehydration. In a subsequent study by Hong and co-workers, it was shown that a solid solution of ECR-40 and the MEI-type aluminosilicate UZM-22 can be formed through an appropriate tuning of the synthesis conditions.[34]

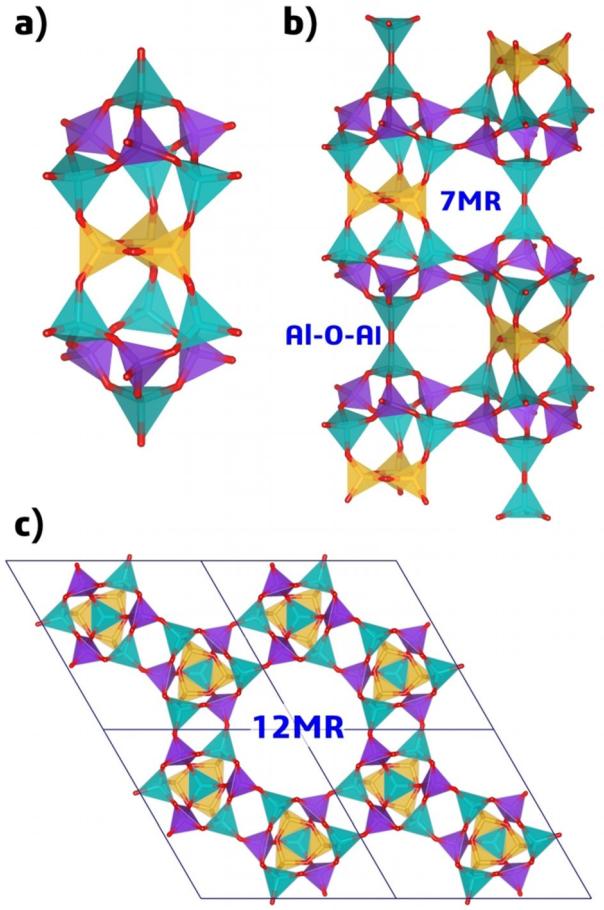

Figure 1. Structure of ECR-40: a) 17 T atom unit, assembled from two $3^1{\cdot}4^3{\cdot}5^3$ building units. b) Two adjacent chains of 17 T atom units running parallel to the *c*-axis. c) Projection of the structure along the *c*-axis. Yellow = silicon, purple = phosphorus, turquoise = aluminium. Structure figures were prepared using VESTA.[35]

The crystal structure of calcined ECR-40, which was refined from synchrotron powder diffraction data, is shown in Figure 2.[29] Each unit cell (u.c.) contains 16 Al, 6 Si, 12 P, and 68 O atoms, leading to a negative framework charge of −4 e/u.c. that needs to be balanced by framework protons. Two likely proton environments can be distinguished: On the one hand, protons can be bonded to the O10 atoms, which form the Si-O-Al linkages (H[O10]). While there are twelve O10

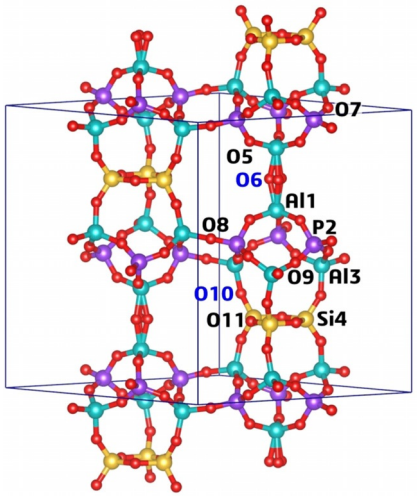

Figure 2. Crystal structure of calcined ECR-40. The atom labelling follows the experimental crystal structure refinement by Afeworki et al.[29] The labelling Scheme used for the MEI framework in the IZA database,[31] which differs from that employed by Afeworki et al., is included in the Supporting Information, Table S1.

atoms per unit cell, at most four of them can be protonated (occupancy of the proton position = 1/3). On the other hand, protons could be located at the O6 atoms, the central atoms of the non-Löwenstein Al-O-Al linkages (H[O6]). However, there are only two O6 atoms per unit cell, leading to the necessity to have at least two additional protons associated with Si-O-Al linkages. Consequently, two limiting scenarios can be defined: First, a model in which all four protons are H[O10] protons, and second, a model that contains two H[O6] and two H[O10] protons. ^{1}H NMR experiments have confirmed the presence of two different proton environments, indicating that the second model is the more realistic one.[29] However, it needs to be pointed out that the experimentally observed intensity ratio of the two signals is not 1:1, which shows that the model described above is simplified with respect to the real structure.

Previous DFT studies of the stability of non-Löwenstein linkages in aluminosilicates had to use computer-generated models assuming different Al distributions. ECR-40 is a rare example of a zeotype where the crystallographic evidence for Al-O-Al linkages is unequivocal, rendering this system particularly interesting from a fundamental point of view, and therefore well suited for a computational study. In this article, dispersion-corrected DFT calculations are employed to study the acidity and mobility of framework protons associated with Al-O-Al and Si-O-Al linkages in ECR-40, aiming at an elucidation of the following aspects:

1. After a full structure optimisation, the total energies of the two models having different proton arrangements are compared to confirm that the model with protonated Al-O-Al linkages is energetically favoured.
2. For this ECR-40(2H[O6], 2H[O10]) model, the acidity of the different protons is investigated by computing the diprotonation energy and studying the interaction with adsorbed molecules (carbon monoxide, ammonia, water).
3. DFT-based molecular dynamics (AIMD) simulations for ECR-40(2H[O6],2H[O10]) at low and high levels of hydration (2 and 38 H_2O molecules/u.c.) are employed to study the dynamic behaviour of ECR-40 in the presence of water, with a particular focus on the potential occurrence of framework deprotonation. Additionally, it is evaluated whether a coordination of water molecules to framework Al atoms occurs, allowing insights into the structural changes upon hydration.

Apart from a thorough computational characterisation of the proton acidity and mobility in the unusual SAPO ECR-40, a material with some potential for acid catalysis, this work also provides further insights into the properties of non-Löwenstein linkages, which have been debated in recent computational studies as outlined above. In particular, Heard et al. hypothesised that their finding of a qualitatively different diprotonation behaviour of Si-O-Al and Al-O-Al linkages, observed for high-silica aluminosilicate zeolites, could be generalised to other protonated zeolites, with the possible exception of high-alumina zeolites with very small pores.[11] Since the present study deals with a silicoaluminophosphate, it permits some conclusions regarding common features and differences between aluminosilicates and aluminophosphates having Al-O-Al linkages.

Models and Methods

Structure models of ECR-40

The initial structure model was taken from the crystal structure of calcined ECR-40 reported by Afeworki et al., who refined the positions of all T and O atoms.[29] This structure is hexagonal, space group $P\frac{6_3}{m}$, with $a = 13.253$ Å and $c = 16.059$ Å (the original publication erroneously reports $c = 15.059$ Å [K. G. Strohmaier, pers. commun.], a corrected CIF file of the experimentally determined crystal structure is supplied as Supporting Information). In this structure, the O6 atom is disordered over three equivalent positions around the sixfold screw axis in order to avoid a linear Al-O-Al linkage (Figure 2). For the calculations, this disorder was removed, leading to a reduction in symmetry to space group $P\frac{2_1}{m}$ (to maintain the relationship to the hexagonal structure, a *c*-unique monoclinic setting was used). Afterwards, the protons were introduced in the manner shown in Figure 3 to generate the ECR-40(2H[O6],2H[O10]) and ECR-40(4H[O10]) models. This was associated with a further reduction in symmetry to space group $P2_1$. For structures including guest molecules, the molecule of interest was placed in the vicinity of either of the two framework protons of ECR-40(2H[O6],2H[O10]), maintaining the $P2_1$ symmetry (thus, there are two guest molecules per unit cell). The experimental saturation water uptake, measured at $T \approx 295$ K and $p/p_0 \approx 0.5$ [K. G. Strohmaier, pers. commun.], amounts to 24.8 wt-%,[29] corresponding to approximately 38 water molecules per unit cell. To construct models of fully hydrated ECR-40, a "pre-covered" model of ECR-40(2H[O6],2H[O10]) in which four water molecules are adsorbed at the framework protons was used as starting point. Initial positions of the remaining 34 H_2O molecules were then obtained from fixed-loading Monte Carlo simulations of water adsorption into this "pre-covered" model. These simulations were performed using the Sorption module of the DS BIOVIA package "Materials Studio", employing the consistent valence force field (CVFF)[36] and a temperature

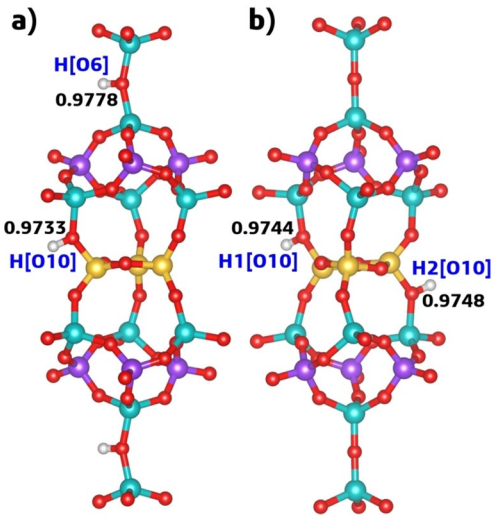

Figure 3. Location of framework protons in a) ECR-40(2H[O6],2H[O10]) and b) ECR-40(4H[O10]). O–H bond lengths of the PBE-TS optimised structures are given in Å.

of 298 K. An analogous strategy was used previously in other computational studies of hydrated SAPOs and AlPOs.[37,38]

Computational methods

The DFT structure optimisations reported in this work were performed with the CASTEP code, version 17.2, which uses a combination of plane waves and pseudopotentials.[39] The calculations used the PBE exchange-correlation functional[40] in conjunction with the dispersion correction devised by Tkatchenko and Scheffler (PBE-TS).[41] Although PBE-based approaches are known to underestimate the length of strong hydrogen bonds and to overstructure bulk water,[42–44] the PBE-TS functional has been used previously with considerable success in studies of guest-free, OSDA-containing, and hydrated AlPOs and SAPOs.[37,38,45–48] The energy cutoff was set to 1000 eV, and only the Γ point was used to sample the first Brillouin zone. Core electrons were represented using norm-conserving pseudopotentials from the Bennett–Rappe database.[49,50] Phonon calculations were performed in the framework of density functional perturbation theory (DFPT).[51] Calculations of the ^{1}H NMR shifts used the gauge including projector augmented waves (GIPAW) method.[52,53] These calculations largely used the same settings as described above, but employed on-the-fly generated ultrasoft pseudopotentials, as the GIPAW method is not implemented for norm-conserving pseudopotentials in CASTEP.

To compare the different proton arrangements, full structure optimisations of guest-free models of ECR-40(2H[O6],2H[O10]) and ECR-40(4H[O6]) were performed. These optimisations included the lattice parameters, but constrained the unit cell to a hexagonal metric ($a=b$, $\alpha=\beta=90^\circ$, $\gamma=120^\circ$). All following calculations focussed on ECR-40(2H[O6],2H[O10]), and used the PBE-TS lattice parameters obtained for the guest-free model. This approximation appears justified, as the differences between the experimental lattice parameters of calcined and hydrated ECR-40 are fairly small, with a differing by around 1.5% and c differing by less than 0.5%.[33] For models of ECR-40(2H[O6],2H[O10]) containing two guest molecules X (X = H_2O, CO, NH_3) at either of the proton sites, the adsorption energy was calculated for the optimised structure according to Equation (1):

$$\Delta E_{ads} = [E_{DFT}(\mathrm{ECR}-40+X) - E_{DFT}(\mathrm{ECR}-40) - 2E_{DFT}(X)]/2 \quad (1)$$

Here, the first and second term on the right-hand side correspond to the PBE-TS energy of ECR-40 with adsorbed guest molecules and of guest-free ECR-40, respectively. The third term corresponds to the total energy of an isolated guest molecule X, obtained from calculations for this molecule in a box with an edge length of 15 Å. In order to obtain the adsorption enthalpy ΔH_{ads} at 298 K, the zero-point vibrational energy (ZPVE) and temperature contributions as obtained from the DFPT phonon calculations were added to each term on the right-hand side, and RT ($\approx$2.5 kJ mol^{-1}) was subtracted from the resulting value.

The AIMD simulations used the CP2K code (version 4.1 installed on the HLRN supercomputer "Konrad"), which is optimised for electronic structure calculations of mid-sized and large systems.[54,55] These simulations were performed in the *NVT* ensemble (T = 298 K) with a Nosé–Hoover thermostat, a time step of 0.5 fs, and a time constant of 50 fs. Due to the unavailability of the TS dispersion correction in CP2K, the AIMD calculations used the "Grimme-type" D3 correction in conjunction with the PBE functional.[40,56] Several previous AIMD studies of hydrated zeolites and zeotypes have employed similar "flavours" of dispersion-corrected DFT.[11,47,57–59] The calculations used a DZVP (double-zeta) basis from the "MOLOPT" basis set included in the current distribution of CP2K[60] and Goedecker–Teter–Hutter pseudopotentials devised by Krack.[61]

Each AIMD trajectory consisted of 20000 steps (= 10 ps), of which the first 5000 steps were used for equilibration. The remaining "production" part of the trajectory was then analysed using the VMD code, the focus being on average structures and, most prominently, radial distribution functions (RDFs).[62] Because the analysis with VMD requires an orthogonal cell, an orthogonal supercell was used in the AIMD calculations. This cell has twice the volume of the hexagonal unit cell. The relationship between both cells is shown in the Supporting Information (Figure S2). AIMD simulations were performed for the guest-free structure of ECR-40(2H[O6],2H[O10]) (as reference), and structures with two water molecules per unit cell (= four per supercell) adsorbed at either of the two framework protons. Three independent AIMD trajectories were calculated to improve the statistics, and all RDFs presented in the following were obtained as an average of the RDFs calculated for the three individual trajectories. For fully hydrated ECR-40, five different snapshots were extracted from the MC simulations described above, and one MD simulation was run starting from each snapshot. Again, the RDFs correspond to averages over the five trajectories.

Results and Discussion

Structure of guest-free ECR-40

Some key results of the calculations for the two different models of guest-free ECR-40 are summarised in Table 1. The ECR-40(2H[O6],2H[O10]) model is energetically favoured by 0.666 eV per unit cell. As the two models differ only in the position of two protons per unit cell (the other two protons are always bonded to O10 atoms), this translates into an energy difference of -32.1 kJ mol^{-1} per proton. This value is roughly an order of magnitude larger than the thermal energy at room temperature, indicating a near-complete occupation of the H[O6] site at any temperature of interest. The relative instabili-

ty of the model with unprotonated Al1-O6-Al1 linkage can be understood when looking at the CASTEP Hirshfeld charges: While the charges at the oxygen atoms in ECR-40(2H[O6],2H[O10]) range from −0.18 to −0.36 e, a significantly more negative value of −0.45 e is found for the O6 atoms in ECR-40(4H[O10]). Apparently, there is a local accumulation of negative charge at these linkages, explaining their higher affinity towards protonation.

The lattice parameter *a* of both models is essentially identical, being about 1% longer than the experimental value (13.39 vs. 13.25 Å). Such moderate overestimations are not uncommon in PBE-TS calculations for aluminophosphate-based materials.[45] On the other hand, the lattice parameter *c* of the ECR-40(2H[O6],2H[O10]) model lies much closer to the experimental value than that of ECR-40(4H[O10]). Even more dramatic differences are observed when looking at the Al-O-Al linkage: If a proton is bonded to the O6 atom, the predicted Al1—O6 bond distance and Al1-O6-Al6 angle agree very well with the experimental values. On the other hand, the optimised ECR-40(4H[O10]) model has an almost linear Al1-O6-Al1 linkage, with the Al1-O6 bonds being around 0.13 Å shorter than in the experimental structure. The O—H bond lengths are included in Figure 3. For the protons associated with the O10 atom, the bond lengths are always close to 0.974 Å, in agreement with previous PBE-TS calculations on SAPOs.[37,38] The O6—H[O6] bond is slightly, but significantly, longer, with 0.978 Å. Interestingly, the opposite trend was observed in the computational study of non-Löwenstein linkages in the aluminosilicate chabazite, where the O—H bond associated with the Al-O-Al linkage was found to be somewhat shorter than those associated with Si-O-Al linkages.[11]

Table 1. Total energies and selected structure parameters obtained from PBE-TS calculations for two models of ECR-40. Experimental structure parameters are given for comparison.[29]

ECR-40 model	PBE-TS 2H[O6], 2H[O10]	PBE-TS 4H[O10]	Experiment
E_{DFT} per u.c. [eV]	−33207.123	−33206.457	
a [Å]	13.392	13.390	13.253
c [Å]	16.166	16.266	16.059
d(Al1—O6) [Å]	1.832	1.684	1.810
α(Al1-O6-Al1) [Å]	154.4	177.5	155.3

To further check the plausibility of the ECR-40(2H[O6],2H[O10]) structure, the ^{1}H NMR shifts were calculated for both models. Experimentally, two signals at 3.3 ppm and 4.3 ppm were attributed to the framework protons associated with Si-O-Al and Al-O-Al linkages, respectively (a third signal was explained with incomplete template removal).[29] While a prediction of the absolute shift values would require a referencing against experimental data,[63] the relative difference between the calculated ^{1}H NMR shifts is sufficient in this context. For ECR-40(2H[O6],2H[O10]) model, the values obtained for the H[O6] and H[O10] protons are indeed ≈1 ppm apart, amounting to 27.7 and 26.7 ppm, respectively. In contrast, the ^{1}H NMR shifts calculated for ECR-40(4H[O10]) are essentially identical (26.5 ppm). The former model thus provides much better agreement with experimental NMR data, corroborating the conclusion drawn from the total energies.

Due to the significant difference in the O—H bond length, the H[O6] and H[O10] protons can also be distinguished by means of vibrational spectroscopy. The computed Raman spectra for the two different models of ECR-40 are shown in the Supporting Information (Figure S1). The spectrum of ECR-40(4H[O10]) has only one band in the O—H stretching region at a frequency of about 3540 cm^{-1}. In the other model, the H[O6] protons give rise to a band at 3500 cm^{-1}, in addition to the H[O10] band at 3550 cm^{-1}. Since these two bands are well separated, it should be possible to resolve them experimentally, and vibrational spectroscopy could be used as an additional tool to distinguish the different proton environments in ECR-40 (and possibly give some semi-quantitative information about their relative amounts).

Deprotonation energy and interaction with adsorbed molecules

Having established that H[O6] and H[O10] protons coexist in ECR-40, it is insightful to investigate to what extent the different environments lead to differences in Brønsted acidity. As a first measure of the acidity, deprotonation energies were computed by means of PBE-TS calculations for negatively charged models in which a single proton of either type was removed. The energy difference with respect to ECR-40(2H[O6],2H[O10]) was then taken as an approximation of the deprotonation energy, following the approach used in previous computational studies of aluminosilicate zeolites and SAPOs.[64–66] Deprotonation of the O6 site gives a deprotonation energy of 1327 kJ mol^{-1}, whereas removal of the H[O10] proton results in a deprotonation energy of 1309 kJ mol^{-1}. While the difference of 18 kJ mol^{-1} is relatively modest, these calculations indicate a higher acidity of the proton associated with the Si-O-Al linkage, in line with the findings of Heard et al. for H-CHA.[11] A reasonably similar deprotonation energy of 1276 kJ mol^{-1} has been reported by Sauer and co-workers for SAPO-34, which contains only Si-O-Al linkages (as these authors used the BLYP functional, the values are not directly comparable).[66]

Both the carbon monoxide adsorption energy and the red-shift of the O—H stretching frequency upon CO adsorption are typically correlated with the acidity.[65,67–70] Therefore, an investigation of CO adsorption at the two different protons represents a complementary means to assess the acidity of the framework protons. Since the quantitative inaccuracies of PBE-based approaches in capturing the interaction of CO with zeolite framework protons have been well documented,[68–70] the interpretation of the results remains largely qualitative. Figure 4 shows the CO adsorption complexes. In both cases, the CO molecule resides above the ring plane, with an essentially linear coordination to the Brønsted acid site. The H_{fw}···C[CO] (fw = framework) distances of 1.9 to 2 Å are in good correspondence with those reported in recent DFT studies of CO adsorption in aluminosilicates.[69,70] The coordination of CO

leads to a significant elongation of the O–H bond to 1.00 Å. As summarised in Table 2, the interaction energy obtained for CO adsorption at the H[O10] proton is only 2 kJ mol^{-1} more negative than for the CO@H[O6] case. The non-dispersive contributions, which mostly stem from the local interaction between the CO molecule and the Brønsted acid site, differ by a more substantial 5 kJ mol^{-1}, in line with the shorter H_{fw}···C[CO] distance. Upon CO adsorption at the H[O6] proton, the C–O stretching frequency increases from 2098 cm^{-1} (uncorrected PBE-TS value obtained from calculations for a CO molecule in a box) to 2146 cm^{-1}. The blueshift obtained for adsorption at the H[O10] proton is very similar, with a frequency of

Table 2. PBE-TS adsorption energies ΔE_{ads}, non-dispersive contribution to adsorption energies, and adsorption enthalpies ΔH_{ads} at $T = 298$ K for CO, NH_3, and H_2O adsorbed at different proton sites of ECR-40(2H[O6],2H[O10]).

	ΔE_{ads} [kJ mol^{-1}]	$\Delta E_{ads,non\text{-}disp}$ [kJ mol^{-1}]	ΔH_{ads}(298 K) [kJ mol^{-1}]
CO@H[O6]	−40.8	−18.9	−38.3
CO@H[O10]	−43.0	−23.7	−40.3
NH_3@H[O6]	−154.9	−129.4	−141.5
NH_3@H[O10]	−150.8	−128.1	−138.6
H_2O@H[O6]	−92.9	−72.9	−90.7
H_2O@H[O10]	−87.4	−68.4	−85.8

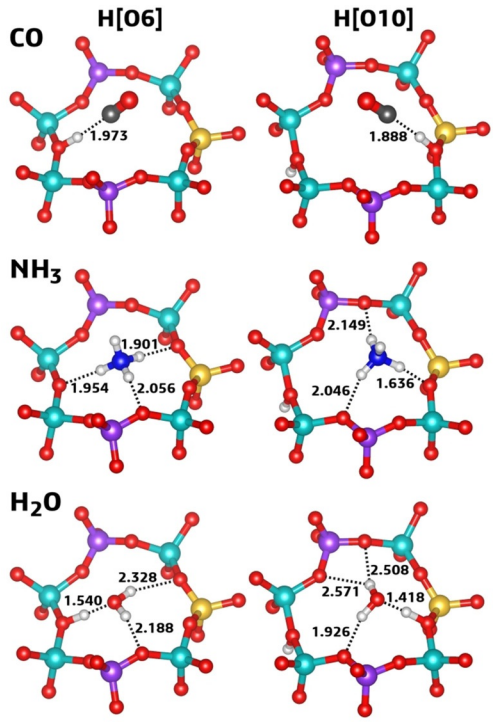

Figure 4. Local environment of DFT-optimised adsorption complexes. In each case, the surrounding 7MR window is shown. Selected framework-guest distances (in Å) are included.

2143 cm^{-1}. With regard to the O–H stretching mode, the redshift upon adsorption amounts to −419 cm^{-1} for H[O6] and to −517 cm^{-1} for H[O10]. The stronger interaction and larger redshift obtained for the CO@H[O10] complex confirm the higher Brønsted acidity of the H[O10] proton, agreeing with the deprotonation energies.

The adsorption of ammonia as a strongly basic molecule is a commonly used technique to characterise the acidity of zeolites, and previous works combining temperature-programmed NH_3 desorption experiments and DFT calculations of the adsorption energy usually found good agreement between experiment and theory on a semi-quantitative level.[71,72] Due to its strong basicity, ammonia is protonated upon interaction with Brønsted acid sites.[69] As is visible in Figure 4, diprotonation of the framework occurs for both the H[O6] and the H[O10] proton, leading to the formation of NH_4^+ cations that are hydrogen-bonded to three framework oxygen atoms. In other words, the acidities of the two protons are not sufficiently different to cause a qualitatively different behaviour upon ammonia adsorption, although there are some differences in the hydrogen bonding pattern (three H-bonds of similar length for H[O6], one short and two longer bonds for H[O10]). The interaction energy is roughly 5 kJ mol^{-1} more negative for adsorption at the H[O6] proton, however, the non-dispersive contribution is very similar for both proton sites. The fact that the results for ammonia do not reproduce the trend in acidity developed above on the basis of deprotonation energies and CO adsorption can be explained using arguments brought forward in the recent literature:[64,69] For ammonia adsorption, the interaction strength is not only determined by the thermodynamics of the proton transfer process, but it also has a significant contribution from attractive interactions between the NH_4^+ cation and framework oxygen atoms. Clear evidence for such interactions is given by the short $H[NH_4^+]$···O_{fw} contacts shown in Figure 4. Hence, no strict correlation between the ammonia adsorption energy and proton acidity can be expected. From a quantitative point of view, the calculated adsorption enthalpies of −140 kJ mol^{-1} are more negative than experimental values obtained for other SAPOs, which typically fall between −105 and −130 kJ mol^{-1}.[71,72] This deviation is likely due to an overestimation of the hydrogen bond strength by the PBE functional.

For the case of water, the adsorption energy amounts to −93 and −88 kJ mol^{-1} for H_2O@H[O6] and H_2O@H[O10], respectively. In a previous PBE-TS study of different SAPOs, interaction energies between −74 and −102 kJ mol^{-1} were obtained, with the interaction strength depending on the local environment of the framework proton.[38] In that previous work, the strongest adsorption sites were found inside 8MR windows. As shown in Figure 4, the water molecule sits above the 7MR windows in ECR-40, participating in a very short hydrogen bond to the framework proton (H_2O as H-bond acceptor) and in two/three longer hydrogen bonds to oxygen atoms (H_2O as H-bond donor). It is noteworthy that there is no obvious correlation between the length of the hydrogen bonds and the adsorption energy. Although the stronger interaction is found for the less acidic H[O6] proton, the elongation of the O_{fw}–H_{fw} bond upon H_2O adsorption is more pronounced for H[O10]: While the O6–H[O6] bond is elongated by 0.07 Å, the

elongation of the O10–H[O10] bond amounts to 0.11 Å. This points to a smaller energetic penalty for an elongation of the O10–H[O10] bond, that is, a weaker bond, which is responsible for the higher acidity of the H[O10] proton.

AIMD simulations: Insights into proton mobility and hydration-induced structural changes

The analysis of the AIMD simulations for guest-free and hydrated models of ECR-40(2H[O6],2H[O10]) consisted of the following steps: First, the average structure calculated from the production part of a given trajectory, as well as the last frame from each trajectory, were visualised in order to get a qualitative overview, for example, to assess whether framework deprotonation or other structural changes had occurred during the AIMD simulation. Average structures and last frames are visualised in Figure S3 to S6 and S7 to S10, respectively. Following this preliminary analysis, selected radial distribution functions (RDFs) *g(r)* as well as cumulative RDFs (integrated *g(r)*) were calculated and analysed to obtain a more quantitative picture.

Guest-free ECR-40

For the model of ECR-40(2H[O6],2H[O10]) without adsorbed water molecules, the AIMD average structures and last frames (Figures S3 and S7) do not deliver any indications for a significant displacement of the framework protons from their starting positions. However, the O6 atom and the attached proton are in some instances found to displace within the plane perpendicular to the Al1-O6-Al1 linkage, indicating that the disorder visualised in Figure 2 is of a dynamic nature. The O–H RDFs, which are displayed in Figure 5, show an oscillation about the equilibrium bond distance of $\approx$0.97 Å without any occurrence of O–H distances $>$1.1 Å, corroborating that the protons are immobile in the guest-free system at this temperature, at least on the picosecond timescale.

ECR-40 with 2 H_2O/u.c.

For ECR-40 models having water molecules adsorbed at either the H[O6] or the H[O10] protons, the average structures and last frames obtained from the AIMD simulations are shown in Figures S4/S5 and S8/S9. While the water molecules are, in a few cases, somewhat displaced from their starting positions, they remain hydrogen-bonded to the framework protons. Previous experimental and computational studies of water adsorption in H-CHA and H-SAPO-34 agreed that the interaction of a single water molecule with Brønsted acid sites does not lead to proton abstraction and formation of a H_3O^+ ion in the pores, whereas interaction with several water molecules can cause framework deprotonation.[11,73–76] This is largely confirmed for ECR-40, where the H_{fw}···O[H_2O] RDFs show maxima at 1.5 Å, corresponding to strong hydrogen bonds (Figure 6). For the H[O10] protons, however, a small secondary maximum centred at a distance of 0.98 Å is visible, indicating the formation of hydronium ions, albeit with low probability. The integrated RDF at a distance of 1.1 Å amounts to 0.003, meaning that a covalent bond between an H[O10] proton and a water oxygen atom is present during only 0.3% of the total simulation time. There are two possible explanations for this observation: On the one hand, the formation of a hydronium ion could occur with a certain probability as a short-lived metastable state, quickly reverting to a hydrogen-bonded water molecule. On the other hand, the proton abstraction could lead to a thermodynamically stable structure, but happen on a much

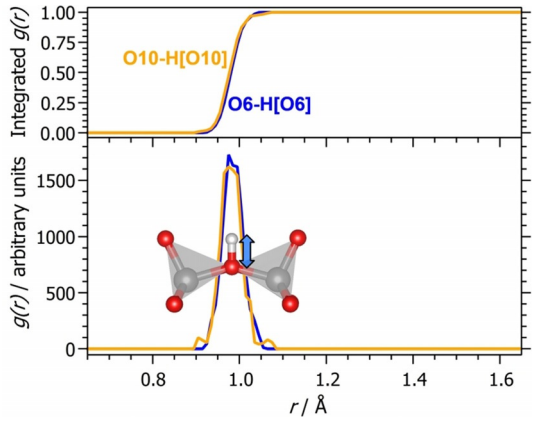

Figure 5. O6–H[O6] and O10–H[O10] RDFs for guest-free ECR-40. The top part of the graph shows the integrated RDFs. In the inset, T atoms are displayed in grey to encompass both Si and Al.

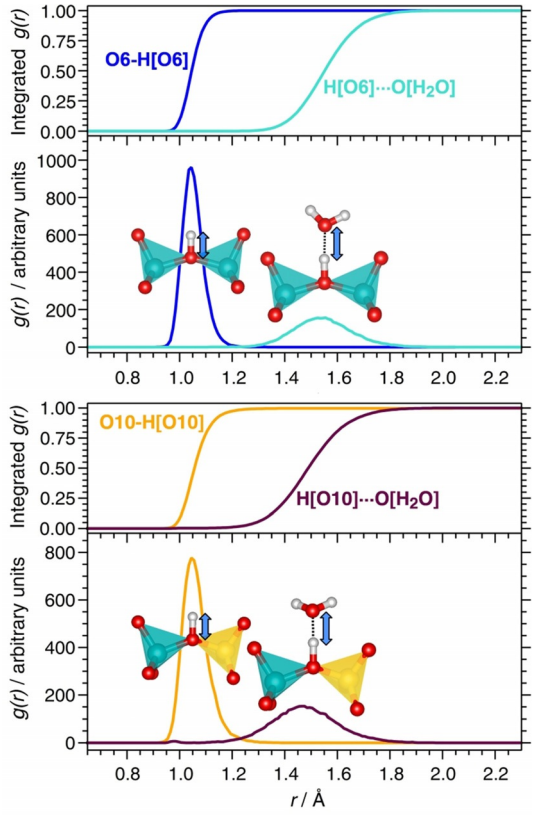

Figure 6. O_{fw}-H_{fw} and H_{fw}···O[H_2O] RDFs for ECR-40 with H_2O molecules adsorbed at the H[O6] protons (top) or at the H[O10] protons (bottom). The top part of each graph shows the integrated RDFs.

longer timescale than the few picoseconds captured by the AIMD simulations. In the latter case, an H_3O^+ ion should be found in at least one of the last frames of the three trajectories, however, this is not observed (Figure S9). The H[O10]···O[H_2O] distances found in the last frames are in the typical range of hydrogen bonds (between 1.35 to 1.58 Å), indicating that the formation of a hydronium ion upon interaction with a single water molecule is indeed a short-lived phenomenon.

ECR-40 with 38 H_2O/u.c.

For fully hydrated ECR-40, the AIMD average structures and last frames are shown in the Supporting Information, Figures S6 and S10. As a number of interesting observations can be made, they will be discussed sequentially, starting with the deprotonation behaviour of the H[O10] protons, continuing with the H[O6] protons, and then looking at structural changes occurring in the environment of framework Al atoms. An inspection of Figure S6 shows that the H[O10] protons are always removed from their initial positions at the framework oxygen atoms and are now bonded to water molecules in the pores (shown exemplarily in Figure 7). As a consequence, hydronium ions or other protonated water clusters (e.g., $H_5O_2^+$ dimers) can be found in the last AIMD frames. The qualitative observation of framework deprotonation is substantiated when looking at the O10-H[O10] RDF, shown in Figure 8. The first non-zero values appear at distances of around 1.5 Å, in the range of hydrogen bonds, well above the covalent O_{fw}–H_{fw} bond length of 1 Å. A sharp maximum in this distance range appears in the RDF between the H[O10] proton and oxygen atoms belonging to any water molecule. The integrated H[O10]···O[H_2O] RDF reaches a value of one at a distance of 1.2 Å, meaning that the probability to find the proton within this distance of one water oxygen atom is 100%. This confirms that the framework deprotonation happens quantitatively. While the removal of the H[O10] protons from their initial positions is thus evident, it could be hypothesised that other protons might, at least with a certain probability, move back from a hydrated hydronium ion in the pores to any unprotonated framework oxygen atom. In order to test whether this occurs, the O–H RDF between all framework oxygen atoms except O6 and all hydrogen atoms was calculated (the environment of O6 will be discussed separately below). This RDF, shown in Figure S11, equals zero at distances below 1.4 Å, that is, there are no protons bonded to framework oxygen atoms of these T-O-T linkages (Si-O-Al, Al-O-P, Si-O-Si). An essentially complete diprotonation of Si-O-Al linkages at high levels of hydration was observed in previous AIMD studies of zeolites and SAPOs.[11,57,58]

We now turn our attention to the H[O6] protons. Here, the picture arising from the average structures is more ambiguous: A significant number of the H[O6] protons are found close to their original positions at the O6 atoms without any significant changes in the local environment (Figure 7). However, some Al1-O6-Al1 linkages are deprotonated. In other cases, significant structural changes occur, such as a coordination of OH groups or water molecules to the Al1 atoms, leading to situations in which two adjacent Al1 atoms are bridged by two or three oxygen atoms (Figure 9). As these changes in the Al coordination environment warrant a separate discussion, the analysis will first focus on the bonding situation of the H[O6] proton. The O6-H[O6] RDF, shown in Figure 8, exhibits a sharp

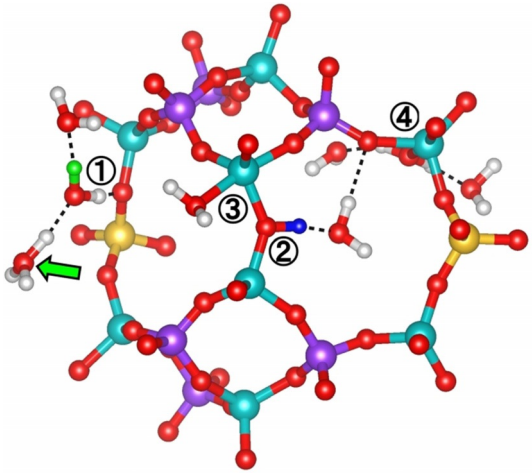

Figure 7. Representative visualisation of key events happening during an AIMD simulation of fully hydrated ECR-40: (1) Removal of H[O10] (green) from the framework, formation of H_3O^+ ion in the vicinity (arrow). (2) No removal of H[O6] (blue). (3) Coordination of water molecule to framework Al1 atom. (4) Coordination of water molecule to framework Al3 atom. The Figure was prepared from the last frame of one AIMD trajectory. For clarity, only a portion of framework and adsorbed water molecules are shown.

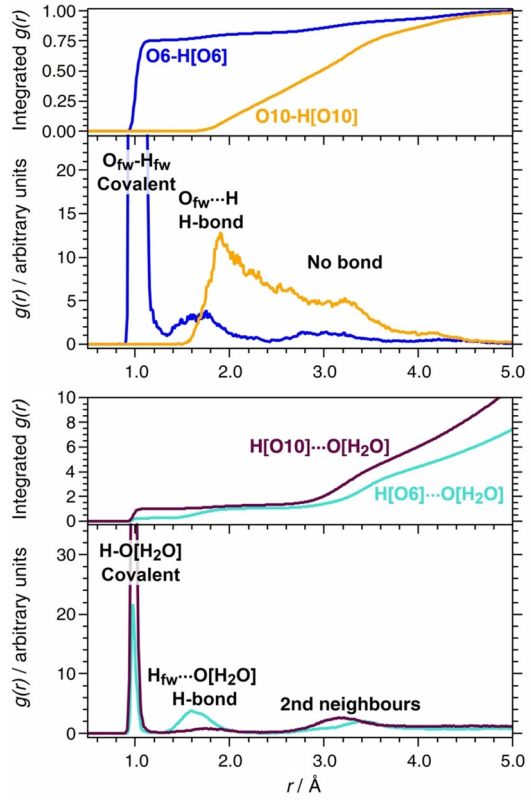

Figure 8. O_{fw}–H_{fw} (top) and H_{fw}···O[H_2O] (bottom) RDFs for fully hydrated ECR-40.

maximum in the distance range of covalent O–H bonds, and the cumulative RDF amounts to 0.75 at a distance of 1.2 Å, indicating that on average, three quarters of the Al1-O6-Al1 linkages remain protonated during the AIMD simulations. Correspondingly, both maxima for covalent O–H bonds and for hydrogen bonds from the H[O6] protons to water oxygen atoms are visible in the H[O6]···O[H_2O] RDF. Altogether, this indicates that the deprotonation of Al-O-Al linkages in ECR-40 does not happen quantitatively as for the Si-O-Al linkages, but that it may occur with a certain probability. Again, there are now two possible scenarios: On the one hand, the protonation of 75% of the Al-O-Al linkages could represent the equilibrium at the simulated temperature. On the other hand, the deprotonation might happen on a much longer timescale than for the Si-O-Al linkages, and thus not be complete after the short simulation time of 10 ps. While a complete elucidation would require much longer simulations, some insights can be gained by calculating the O6–H[O6] RDF for different parts of the whole production stage. This was done by dividing the production stage into three segments with a length of 2.5 ps each (Figure S12). The differences between the integrated RDFs of the three segments are only intricate. Moreover, 75% of the Al1-O6-Al1 linkages are protonated in the last AIMD frames. Altogether, it can thus be concluded that the deprotonation occurred during the first 2.5 ps of equilibration, without a significant number of deprotonation or reprotonation events happening over the course of the production stage.

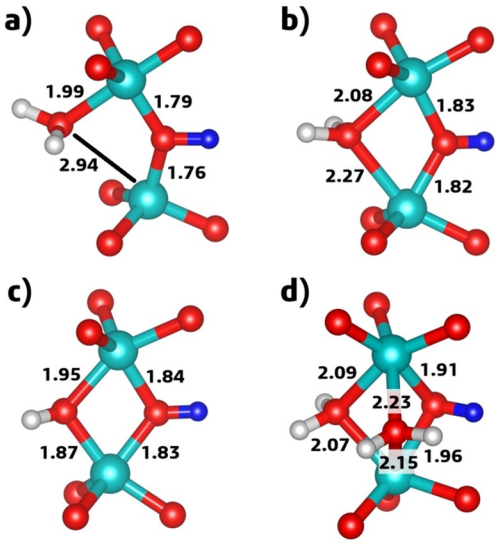

Figure 9. Representative environments of the Al1-O6-Al1 linkage found in last frames of the AIMD trajectories. a) Coordination of an H_2O molecule to an Al1 atom. b) H_2O molecule in a bridging position between two Al1 atoms. c) Two bridging OH groups. d) Octahedrally coordinated Al1 atoms, bonded to one OH group and two H_2O molecules. Al–O distances (in Å) are given for guidance, however, it should be noted that these are not optimised equilibrium distances, but instantaneous values.

In hydrated AlPOs and related materials, water molecules may bond to framework Al atoms, leading to a change in the coordination number of Al to five or six. The formation of such "higher-coordinated" Al atoms has been well established experimentally[77–83] and also been observed in previous DFT studies.[37,38,82–84] An inspection of the AIMD average structures and last frames does indeed show such a formation of Al–O[H_2O] bonds. Changes in the Al coordination environment are—with one exception, discussed below—limited to an increase of the coordination number to five (trigonal bipyramidal coordination). A coordination of water is observed for both the Al1 and the Al3 atoms, and a representative local environment of a water molecule bonded to an Al1 atom is visualised in Figure 9a. In some of the last frames of the AIMD trajectories, more striking structural changes are observed: In these cases, either a water molecule or an OH group are bonded to two neighbouring Al1 atoms, thereby forming a second Al-O-Al "bridge" (Figure 9b,c). This can be interpreted as two phases of a—possibly irreversible—structural change: After a water molecule is initially bonded to a single Al1 atom, thermal motion may displace it towards the equatorial plane of the Al-O-Al linkage, where it can interact with both Al1 atoms simultaneously. Subsequently, a proton is abstracted and moves to one of the surrounding water molecules, resulting in a second bridging OH group. In one particular instance, a further evolution is observed, with two Al1 atoms being bridged by one OH groups and two water molecules (Figure 9d). As a result, both Al1 atoms are octahedrally coordinated, in line with the experimental observation of octahedral Al1 environments in the crystal structure of hydrated ECR-40.[33]

In order to analyse the relative probabilities of the two different Al atoms to expand their coordination numbers beyond four, the Al–O_{fw} and Al–O[H_2O]RDFs were calculated. They are shown in Figure 10. For both Al atoms, a high maximum (not fully shown) is visible in the Al–O_{fw} RDF, which is centred at about 1.80 Å for Al1 and at about 1.76 Å for Al3. The cumulative RDFs reach the expected value of 4 at a distance of around 2 Å, meaning each framework Al atom is surrounded by four O_{fw} atoms. Broader, much smaller maxima appear in the Al–O[H_2O] RDFs, with the highest values being reached at distances of 1.93 Å (Al1) and 2.01 Å (Al3). This maximum is much more prominent for Al1, indicating that a coordination of water molecules to this aluminium atom occurs with higher probability than for Al3. In order to quantify this, the average coordination number of the framework aluminium atoms can be calculated by adding up the integrated Al–O_{fw} and Al–O[H_2O] RDFs at a suitable distance above the first maxima. Using a distance of 2.5 Å delivers an average coordination number of 4.61 for the Al1 atoms, and 4.09 for the Al3 atoms. These results corroborate that the Al1 atoms are much more susceptible towards an expansion of their coordination number, but that coordination of water molecules to the Al3 atoms also occurs to a non-negligible extent.

Discussion

On the basis of the body of results presented above, it can be concluded that protons associated with Si-O-Al linkages in ECR-40 have a higher acidity than those at the Al-O-Al linkages. This trend in acidity is found in the static calculations

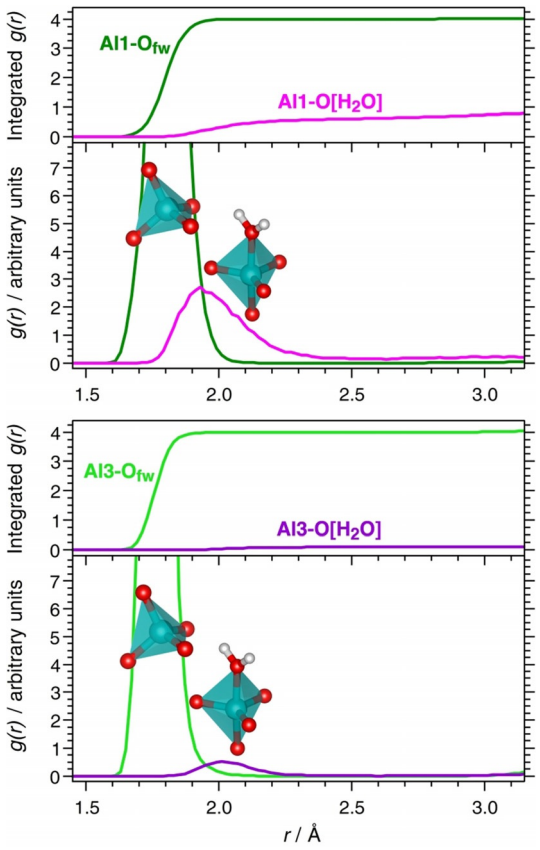

Figure 10. Al–O_{fw} and Al–O[H_2O] RDFs for Al1 (top) and Al3 (bottom) atoms in fully hydrated ECR-40.

(diprotonation energy, CO adsorption complexes) and is corroborated by the different deprotonation behaviour of H[O6] and H[O10] protons in the AIMD simulations of fully hydrated ECR-40. Furthermore, it is confirmed that the NH_3 adsorption energy provides no reliable indicator for the acidity. While all these findings are in line with recent literature reports,[11,64,69] one may note two rather surprising aspects: First, there is usually an inverse correlation between proton acidity and O–H stretching frequency, and the frequency depends on the length of the covalent O–H bond (longer bonds→lower stretching frequency→higher acidity).[65] The opposite is observed here, with the O6–H[O6] bond being about 0.005 Å longer than the O10–H[O10] bond (Figure 3). As a consequence, the more acidic H[O10] proton gives rise to a band at higher frequency than the less acidic H[O6] proton, contrary to the commonly expected relationship. Tentatively, this deviation from the correlation between bond length and bond strength can be attributed to a larger ionic contribution to the O6–H[O6] bond due to the increased negative polarisation of the O6 atom. Second, it is worth pointing out that Afeworki et al. attributed the comparatively high acidity of ECR-40 to two factors:[29] On the one hand, all Si atoms are surrounded by two Al and two Si atoms, which should cause a higher acidity than typical Si(4Al) environments or silicon islands. On the other hand, the authors also suspected that the Al-O-Al linkages could provide highly acidic sites. While the former explanation cannot be verified (or falsified) without a detailed comparison of ECR-40 to other SAPOs at a consistent level of theory, the findings of the present study disagree with the second hypothesis.

Both types of protons in ECR-40 are immobile in the guest-free structure (at least at room temperature and on the timescale of picoseconds), and the interaction of a Brønsted acid site with a single water molecule is not sufficient to cause a removal of the protons from their initial positions. On the other hand, framework deprotonation does occur at high levels of hydration, quantitatively for the more acidic H[O10] protons, and to a non-negligible extent for the less acidic H[O6] protons associated with the non-Löwenstein linkages. The influence of the water content on the extent of deprotonation of Si-O-Al linkages has been investigated in several previous computational studies, and the findings of the present work agree with these results.[11,57,58,74–76] Experimentally, it has also been established that the interaction of each Brønsted acid site with a single water molecule is not sufficient for deprotonation, but that the formation of protonated water clusters occurs upon interaction with larger amounts of water due to cooperative effects.[12,73,85] The hydration behaviour of the H[O10] protons in ECR-40 is thus analogous to that of protons at Si-O-Al linkages in more typical SAPOs and aluminosilicate zeolites. On the other hand, the observed partial deprotonation of Al-O-Al linkages in ECR-40 deviates from the results of Heard et al., who found that these linkages were quickly reprotonated when starting the AIMD simulation from an initial model with hydrated hydronium ions in the pores and no framework protons.[11] Hence, there seems to be a qualitative difference between the deprotonation probability of Al-O-Al linkages in aluminosilicates and the aluminophosphate-based ECR-40. This might indicate that Al-O-Al linkages in aluminosilicates constitute an even more pronounced charge imbalance, rendering their deprotonation thermodynamically more unfavourable, but further computational work would be required to gain more detailed insights. In addition to analysing the occurrence of framework deprotonation as such, it is also interesting to evaluate what happens to the protons after their removal from the framework. As Figure 8 shows, roughly 50% of the H[O10] protons are located at a distance of more than 3 Å from the O10 atom over the course of the AIMD simulation (15% at distances >4 Å), pointing to a significant mobility of the protons within the protonated water clusters.

Along with insights into proton mobility, the calculations also clearly show that adsorbed water molecules can form bonds to framework Al atoms. While the coordination of water to framework Al atoms may happen at both Al positions, the localisation of water in a bridging position between two T atoms occurs only at the Al-O-Al linkages, simply because silicon and phosphorus are much less susceptible to an expansion of their coordination number beyond four. The bridging water molecules tend to be deprotonated, increasing the charge separation between the negatively charged framework and the protonated water clusters. Since the AIMD simulations were run for a few picoseconds, only, it has to be expected that the number of Al–O[H_2O] bonds would increase if a

longer time was covered. It is worth noting that the coordination of water molecules to framework Al atoms has been identified as a crucial first step in computational studies of the desilication of SAPOs[86] and the dealumination of aluminosilicate zeolites.[87,88] Altogether, it appears logical to draw a link between the hydration-induced structural changes at the Al-O-Al linkages in ECR-40, which are detectable even on the timescale of the AIMD simulations, and the experimentally observed instability of hydrated ECR-40 towards recalcination.[33] While the surrounding water molecules are not shown in Figure 9, inspection of the complete AIMD frames shows that the local arrangements shown in the Figure are stabilised through hydrogen bonds to water molecules adsorbed in the pores. If these molecules are removed upon calcination, the stabilising hydrogen bonds are missing, and it is to be expected that those Al-O-Al linkages that have been modified upon hydration will be especially prone to break apart upon dehydration. As the Al-O-Al connections are a key structural element of ECR-40, linking the 17 T atom building units along the *c*-axis, breaking these linkages would lead to a collapse of the long-range order.

Conclusions

The calculations comparing guest-free ECR-40 with two different possible proton arrangements clearly showed an energetic preference for a complete protonation of the non-Löwenstein Al-O-Al linkages, an observation that is explained with the accumulation of a negative excess charge at the O6 atom. As it incurs a larger energetic penalty to remove protons from Al-O-Al linkages than from Si-O-Al linkages, the H[O6] protons possess a lower Brønsted acidity, and they are unlikely to be responsible for the exceptional performance of ECR-40 as acid catalyst in the cracking of *n*-hexane ("alpha test").[29] In the computation of host-guest interaction energies for three guest molecules (CO, NH_3, H_2O), only the results for CO adsorption delivered the trend in acidity established from the diprotonation energies, whereas ammonia and water were found to be unsuitable molecules to probe the acidity (and even for CO, the correlation may be fortuitous[69]).

Due to their lower acidity, the protons at the Al-O-Al linkages are less likely to be removed from their initial positions upon hydration at room temperature. However, deprotonation does occur to a certain extent, as the protonated water clusters in the pores can neutralise the accumulation of negative charge in this part of the framework. In the previous study by Heard et al., it was found that the formation of protonated water clusters provides a stabilising energetic component.[11] As non-Löwenstein linkages remained completely protonated in the aluminosilicate zeolites studied, it was concluded that the formation of these linkages in aqueous media is thermodynamically unfavourable because such a stabilising contribution is missing. Although the difference between protons associated with Si-O-Al and Al-O-Al linkages is less clear-cut in ECR-40, the present work does not invalidate these conclusions. Looking at the problem from another angle, the present results can provide an additional explanation why non-Löwenstein linkages are rarely found in aluminosilicate or (silico)aluminophosphate zeotypes: The observed structural changes in the vicinity of the Al-O-Al linkages of ECR-40 indicate that these linkages are irreversibly modified upon hydration, and prone to break entirely upon water removal. Thus, even in cases where the thermodynamic barrier towards formation of such links may be overcome in the first place, they are less likely to survive the complete formation process. The actual existence of Al-O-Al linkages in ECR-40 is due to the presence of framework-bound OSDA molecules in the as-synthesised structure, a rather unusual situation that is not found in typical zeolite syntheses, let alone natural zeolites.

Supporting Information

Calculated Raman spectra of guest-free ECR-40, additional information and results of AIMD simulations, sample input files, CIF file of experimental crystal structure (with corrected *c* parameter), CIF files of DFT-optimised structures, CIF files of average structures from AIMD simulations, CIF files of last frames from AIMD simulations.

Acknowledgements

This research was funded by the Deutsche Forschungsgemeinschaft (DFG—German Research Foundation), project number 389577027 (FI 1800/5-1). I would like to thank Andreas Lüttge and Rolf S. Arvidson for access to the Asgard cluster, on which the CASTEP calculations were run. The CP2K-AIMD calculations made use of resources provided by the North-German Supercomputing Alliance (HLRN). I am grateful to Karl G. Strohmaier for providing additional information regarding the experimental characterisation of ECR-40. Finally, I am indebted to Frank Hoffmann for a careful and critical reading of a draft version of this article.

Conflict of interest

The authors declare no conflict of interest.

Keywords: density functional calculations · molecular dynamics · proton acidity · silicoaluminophosphates · zeolites

[1] W. Loewenstein, *Am. Mineral.* **1954**, *39*, 92 – 96.
[2] L. Pauling, *J. Am. Chem. Soc.* **1929**, *51*, 1010 – 1026.
[3] J. V. Smith, *Feldspar Minerals 1. Crystal Structure and Physical Properties*, Springer, Berlin **1974**.
[4] L. Peters, N.-S. Rahmoun, K. Knorr, W. Depmeier in *Minerals as Advanced Materials I* (Ed.: S. V. Krivovichev), Springer, Berlin, **2008**, pp. 17 – 25.
[5] T. Armbruster, M. E. Gunter, *Rev. Mineral. Geochem.* **2001**, *45*, 1 – 67.
[6] J. F. Stebbins, P. Zhao, S. K. Lee, X. Cheng, *Am. Mineral.* **1999**, *84*, 1680 – 1684.
[7] X. Cheng, P. Zhao, J. F. Stebbins, *Am. Mineral.* **2000**, *85*, 1030 – 1037.
[8] W. Depmeier, *Phys. Chem. Miner.* **1988**, *15*, 419 – 426.
[9] P. Florian, E. Veron, T. F. G. Green, J. R. Yates, D. Massiot, *Chem. Mater.* **2012**, *24*, 4068 – 4079.
[10] R. E. Fletcher, S. Ling, B. Slater, *Chem. Sci.* **2017**, *8*, 7483 – 7491.
[11] C. J. Heard, L. Grajciar, P. Nachtigall, *Chem. Sci.* **2019**, *10*, 5705 – 5711.

[12] S. Eckstein, P. H. Hintermeier, R. Zhao, E. Baráth, H. Shi, Y. Liu, J. A. Lercher, *Angew. Chem. Int. Ed.* **2019**, *58*, 3450 – 3455; *Angew. Chem.* **2019**, *131*, 3488 – 3493.
[13] S. T. Wilson, *Stud. Surf. Sci. Catal.* **2001**, *137*, 229 – 260.
[14] H. O. Pastore, S. Coluccia, L. Marchese, *Annu. Rev. Mater. Res.* **2005**, *35*, 351 – 395.
[15] J. Yu, R. Xu, *Chem. Soc. Rev.* **2006**, *35*, 593 – 604.
[16] S. Kulprathipanja, *Zeolites in Industrial Separation and Catalysis*, Wiley-VCH, Weinheim, **2010**.
[17] D. Chen, K. Moljord, A. Holmen, *Microporous Mesoporous Mater.* **2012**, *164*, 239 – 250.
[18] P. Tian, Y. Wei, M. Ye, Z. Liu, *ACS Catal.* **2015**, *5*, 1922 – 1938.
[19] Q. Liu, N. C. O. Cheung, A. E. Garcia-Bennett, N. Hedin, *ChemSusChem* **2011**, *4*, 91 – 97.
[20] O. Cheung, Q. Liu, Z. Bacsik, N. Hedin, *Microporous Mesoporous Mater.* **2012**, *156*, 90 – 96.
[21] S. Li, J. L. Falconer, R. D. Noble, *J. Membr. Sci.* **2004**, *241*, 121 – 135.
[22] A. Ristić, N. Zabukovec Logar, S. K. Henninger, V. Kaučič, *Adv. Funct. Mater.* **2012**, *22*, 1952 – 1957.
[23] A. Krajnc, J. Varlec, M. Mazaj, A. Ristić, N. Z. Logar, G. Mali, *Adv. Energy Mater.* **2017**, *7*, 1601815.
[24] G. Sastre, D. W. Lewis, C. R. A. Catlow, *J. Phys. Chem.* **1996**, *100*, 6722 – 6730.
[25] G. Sastre, D. W. Lewis, C. R. A. Catlow, *J. Mol. Catal. A Chem.* **1997**, *119*, 349 – 356.
[26] V. V. Klepov, C. A. Juillerat, E. V. Alekseev, H.-C. zur Loye, *Inorg. Chem.* **2019**, *58*, 724 – 736.
[27] Q. Huang, S. Hwu, *Chem. Commun.* **1999**, 2343 – 2344.
[28] D. E. W. Vaughan, Synthesis of and Composition of ECR-40, Large Pore Aluminophosphate, **1999**, US Patent No. 5976491A.
[29] M. Afeworki, D. L. Dorset, G. J. Kennedy, K. G. Strohmaier, *Stud. Surf. Sci. Catal.* **2004**, *154*, 1274 – 1281.
[30] S. L. Lawton, W. J. Rohrbaugh, *Science* **1990**, *247*, 1319 – 1322.
[31] C. Baerlocher, L. B. McCusker, http://www.iza-structure.org/databases**2018**.
[32] N. A. Anurova, V. A. Blatov, G. D. Ilyushin, D. M. Proserpio, *J. Phys. Chem. C* **2010**, *114*, 10160 – 10170.
[33] J. K. Lee, J. Shin, N. H. Ahn, A. Turrina, M. B. Park, Y. Byun, S. J. Cho, P. A. Wright, S. B. Hong, *Angew. Chem. Int. Ed.* **2015**, *54*, 11097 – 11101; *Angew. Chem.* **2015**, *127*, 11249 – 11253.
[34] J. K. Lee, J. H. Lee, N. H. Ahn, K. H. Cho, S. B. Hong, *Chem. Sci.* **2016**, *7*, 5805 – 5814.
[35] K. Momma, F. Izumi, *J. Appl. Crystallogr.* **2011**, *44*, 1272 – 1276.
[36] J.-R. Hill, A. R. Minihan, E. Wimmer, C. J. Adams, *Phys. Chem. Chem. Phys.* **2000**, *2*, 4255 – 4264.
[37] M. Fischer, *Phys. Chem. Chem. Phys.* **2015**, *17*, 25260 – 25271.
[38] M. Fischer, *Phys. Chem. Chem. Phys.* **2016**, *18*, 15738 – 15750.
[39] S. J. Clark, M. D. Segall, C. J. Pickard, P. J. Hasnip, M. I. J. Probert, K. Refson, M. C. Payne, *Z. Kristallogr.* **2005**, *220*, 567 – 570.
[40] J. P. Perdew, K. Burke, M. Ernzerhof, *Phys. Rev. Lett.* **1996**, *77*, 3865 – 3868.
[41] A. Tkatchenko, M. Scheffler, *Phys. Rev. Lett.* **2009**, *102*, 073005.
[42] J. Ireta, J. Neugebauer, M. Scheffler, *J. Phys. Chem. A* **2004**, *108*, 5692 – 5698.
[43] M. Chen, H.-Y. Ko, R. C. Remsing, M. F. Calegari Andrade, B. Santra, Z. Sun, A. Selloni, R. Car, M. L. Klein, J. P. Perdew, X. Wu, *Proc. Natl. Acad. Sci. USA* **2017**, *114*, 10846 – 10851.
[44] M. J. Gillan, D. Alfè, A. Michaelides, *J. Chem. Phys.* **2016**, *144*, 130901.
[45] M. Fischer, F. O. Evers, F. Formalik, A. Olejniczak, *Theor. Chem. Acc.* **2016**, *135*, 257.
[46] M. Fischer, W. J. Kim, M. Badawi, S. Lebègue, *J. Chem. Phys.* **2019**, *150*, 094102.
[47] M. Fischer, *Molecules* **2019**, *24*, 922.
[48] M. Fischer, *Phys. Chem. Miner.* **2019**, *46*, 385 – 401.
[49] J. W. Bennett, *Phys. Procedia* **2012**, *34*, 14 – 23.
[50] A. M. Rappe, "PBE Pseudopotentials Online Repository" can be found under: https://www.sas.upenn.edu/rappegroup/research/pseudo-potential-gga.html; accessed 02/2019.
[51] K. Refson, P. R. Tulip, S. J. Clark, *Phys. Rev. B* **2006**, *73*, 155114.
[52] C. J. Pickard, F. Mauri, *Phys. Rev. B* **2001**, *63*, 245101.
[53] J. R. Yates, C. J. Pickard, F. Mauri, *Phys. Rev. B* **2007**, *76*, 024401.
[54] J. VandeVondele, M. Krack, F. Mohamed, M. Parrinello, T. Chassaing, J. Hutter, *Comput. Phys. Commun.* **2005**, *167*, 103 – 128.
[55] J. Hutter, M. Iannuzzi, F. Schiffmann, J. VandeVondele, *WIREs Comput. Mol. Sci.* **2014**, *4*, 15 – 25.
[56] S. Grimme, J. Antony, S. Ehrlich, H. Krieg, *J. Chem. Phys.* **2010**, *132*, 154104.
[57] K. De Wispelaere, B. Ensing, A. Ghysels, E. J. Meijer, V. Van Speybroeck, *Chem. Eur. J.* **2015**, *21*, 9385 – 9396.
[58] K. De Wispelaere, C. S. Wondergem, B. Ensing, K. Hemelsoet, E. J. Meijer, B. M. Weckhuysen, V. Van Speybroeck, J. Ruiz-Martínez, *ACS Catal.* **2016**, *6*, 1991 – 2002.
[59] E. Fois, G. Tabacchi, *Z. Kristallogr.* **2019**, *234*, 495 – 511.
[60] J. VandeVondele, J. Hutter, *J. Chem. Phys.* **2007**, *127*, 114105.
[61] M. Krack, *Theor. Chem. Acc.* **2005**, *114*, 145 – 152.
[62] W. Humphrey, A. Dalke, K. Schulten, *J. Mol. Graph.* **1996**, *14*, 33 – 38.
[63] S. E. Ashbrook, D. McKay, *Chem. Commun.* **2016**, *52*, 7186 – 7204.
[64] A. J. Jones, E. Iglesia, *ACS Catal.* **2015**, *5*, 5741 – 5755.
[65] J. Sauer, *Faraday Discuss.* **2016**, *188*, 227 – 234.
[66] J. Sauer, K.-P. Schröder, V. Termath, *Collect. Czechoslov. Chem. Commun.* **1998**, *63*, 1394 – 1408.
[67] P. Nachtigall, O. Bludský, L. Grajciar, D. Nachtigallová, M. R. Delgado, C. O. Areán, *Phys. Chem. Chem. Phys.* **2009**, *11*, 791 – 802.
[68] C. Otero Arean, M. R. Delgado, P. Nachtigall, H. V. Thang, M. Rubeš, R. Bulánek, P. Chlubná-Eliášová, *Phys. Chem. Chem. Phys.* **2014**, *16*, 10129 – 10141.
[69] M. Boronat, A. Corma, *ACS Catal.* **2019**, *9*, 1539 – 1548.
[70] M. Rubeš, M. Trachta, E. Koudelková, R. Bulánek, J. Klimeš, P. Nachtigall, O. Bludský, *J. Phys. Chem. C* **2018**, *122*, 26088 – 26095.
[71] K. Suzuki, T. Nishio, N. Katada, G. Sastre, M. Niwa, *Phys. Chem. Chem. Phys.* **2011**, *13*, 3311 – 3318.
[72] N. Katada, K. Nouno, J. K. Lee, J. Shin, S. B. Hong, M. Niwa, *J. Phys. Chem. C* **2011**, *115*, 22505 – 22513.
[73] S. Bordiga, L. Regli, C. Lamberti, A. Zecchina, M. Bjørgen, K. P. Lillerud, *J. Phys. Chem. B* **2005**, *109*, 7724 – 7732.
[74] V. Termath, F. Haase, J. Sauer, J. Hutter, M. Parrinello, *J. Am. Chem. Soc.* **1998**, *120*, 8512 – 8516.
[75] Y. Jeanvoine, J. G. Ángyán, G. Kresse, J. Hafner, *J. Phys. Chem. B* **1998**, *102*, 7307 – 7310.
[76] M. V. Vener, X. Rozanska, J. Sauer, *Phys. Chem. Chem. Phys.* **2009**, *11*, 1702 – 1712.
[77] C. S. Blackwell, R. L. Patton, *J. Phys. Chem.* **1984**, *88*, 6135 – 6139.
[78] J. J. Pluth, J. V. Smith, *Acta Crystallogr. Sect. C* **1986**, *42*, 1118 – 1120.
[79] L. B. McCusker, C. Baerlocher, E. Jahn, M. Bülow, *Zeolites* **1991**, *11*, 308 – 313.
[80] P.-P. Knops-Gerrits, H. Toufar, X.-Y. Li, P. Grobet, R. A. Schoonheydt, P. A. Jacobs, W. A. Goddard, *J. Phys. Chem. A* **2000**, *104*, 2410 – 2422.
[81] J. Varlec, A. Krajnc, M. Mazaj, A. Ristić, K. Vanatalu, A. Oss, A. Samoson, V. Kaučič, G. Mali, *New J. Chem.* **2016**, *40*, 4178 – 4186.
[82] G. Poulet, P. Sautet, A. Tuel, *J. Phys. Chem. B* **2002**, *106*, 8599 – 8608.
[83] G. Poulet, A. Tuel, P. Sautet, *J. Phys. Chem. B* **2005**, *109*, 22939 – 22946.
[84] E. Fois, A. Gamba, A. Tilocca, *J. Phys. Chem. B* **2002**, *106*, 4806 – 4812.
[85] A. Vjunov, M. Wang, N. Govind, T. Huthwelker, H. Shi, D. Mei, J. L. Fulton, J. A. Lercher, *Chem. Mater.* **2017**, *29*, 9030 – 9042.
[86] T. Fjermestad, S. Svelle, O. Swang, *J. Phys. Chem. C* **2015**, *119*, 2073 – 2085.
[87] M. C. Silaghi, C. Chizallet, J. Sauer, P. Raybaud, *J. Catal.* **2016**, *339*, 242 – 255.
[88] K. Stanciakova, B. Ensing, F. Göltl, R. E. Bulo, B. M. Weckhuysen, *ACS Catal.* **2019**, *9*, 5119 – 5135.

Manuscript received: June 27, 2019
Revised manuscript received: August 21, 2019
Accepted manuscript online: August 23, 2019
Version of record online: September 20, 2019

